THE SPECTRUM OF THE ACOUSTIC WAVES BACKSCATTERED BY THE DYNAMIC ROUGH SURFACE OF A SHALLOW WATER FLOW

G Dolcetti Department of Mechanical Engineering, The University of Sheffield, Sheffield, UK
A Krynkin Department of Mechanical Engineering, The University of Sheffield, Sheffield, UK
KV Horoshenkov Department of Mechanical Engineering, The University of Sheffield, Sheffield, UK
SJ Tait Department of Civil and Structural Engineering, The University of Sheffield, Sheffield, UK

1 INTRODUCTION

Scattering of airborne ultrasonic waves by the moving rough surface of a shallow water flow is a poorly explored topic. In particular, acoustic wave scattering from the free-surface of shallow water flows such as rivers or open-channels has been relatively neglected. Most of the existing studies focus on backscattering from the ocean surface, where Doppler spectra have been used to recover useful information on the wind-generated waves[1]. These works are based largely on electromagnetic waves. For flows in hydraulically narrow, prismatic channels it is expected that the surface roughness is generated mainly by the action of turbulence inside the water flow, and the roughness pattern is largely two-dimensional and dominated by the dispersive nature of waves. The existing studies on shallow flows are limited to the measurement of the Doppler spectra of backscattered electromagnetic waves with the aim of determining the velocity of the flow[2,3,4,5]. In this paper we will show how the analysis of Doppler spectra of airborne ultrasonic backscattered waves could be used in order to obtain useful information on the characteristics of the turbulence-driven surface roughness and its dynamics, which could eventually improve our understanding of the interaction between turbulence and the free-surface in a turbulent, open channel flow.

2 BACKSCATTERING FROM THE WATER FREE-SURFACE

2.1 Scattering from a rough moving surface

When airborne acoustic waves interact with a rough surface they are scattered in a way that depends on the geometric characteristics of the surface. We consider scattering from an ideal rigid 2-dimensional surface Σ dynamically perturbed around its equilibrium state Σ_0 which coincides with the x-axis. The surface elevation is represented by a smooth random homogeneous function $\zeta(x,t)$ of the single spatial variable x and time t which average is zero and which standard deviation is $\sigma = \sqrt{<\zeta^2(x,t)>}$, where the symbol <> stands for ensemble averaging over time. Considering acoustic waves propagating at a certain angle ψ with respect to Σ_0 so that shadowing and multiple scattering effects can be neglected, the reflection from the rough surface at each point can be approximated by the single reflection from a tangent plane to the surface provided[6]

$$sin\psi \gg \frac{1}{\sqrt[3]{k_0 a}} \quad , \tag{1}$$

where k_0 is the wavenumber of the acoustic wave and a is the curvature radius of the surface at the point of reflection.

Let us assume that the position of the acoustic source and receiver are identified by vectors $\boldsymbol{S}$ and $\boldsymbol{M}$, the position of the rough surface is described by the vector $\boldsymbol{r}(t) = \big(x, \zeta(x,t)\big)$ and the path of the acoustic wave from the source S to a point r on the surface and from the point r to the receiver M is

described by the vectors $\boldsymbol{R_S} = \boldsymbol{r} - \boldsymbol{S}$ and $\boldsymbol{R_M} = \boldsymbol{M} - \boldsymbol{r}$, respectively. The direction of these vectors also defines the incident and reflected wavenumbers $\boldsymbol{k_S} = k_0\boldsymbol{R_S}/|\boldsymbol{R_S}|$ and $\boldsymbol{k_M} = k_0\boldsymbol{R_M}/|\boldsymbol{R_M}|$, respectively. By only considering waves propagating along the plane (x, z) the wavenumber variation due to the reflection at the surface is $\boldsymbol{q} = \boldsymbol{k_M} - \boldsymbol{k_S} = q_x\boldsymbol{i_x} + q_z\boldsymbol{i_z}$. The rough surface is in the far field with respect to both the source and the receiver ($k_0R_S \gg 1$, $k_0R_M \gg 1$), then the source can be modelled as a point source and the scattered acoustic field at point M can be written as[6]

$$U(\boldsymbol{M},\boldsymbol{S},t) = \Lambda\,\delta(q_y)\frac{e^{-i\omega_0 t}}{i4\pi}\int_{\Sigma}\frac{D_S(x,t)D_M(x,t)}{R_S(x,t)R_M(x,t)}e^{ik_0[R_S(x,t)+R_M(x,t)]}\boldsymbol{q}(x,t)\cdot[\boldsymbol{i_z} - \eta(x,t)\boldsymbol{i_x}]dx \quad , \quad (2)$$

where D_S and D_M represent the directivity patterns of the source and of the receiver respectively, for the radian frequency ω_0, $\eta = \partial\zeta/\partial x$ is the spatial gradient of the rough surface at point x, $\delta(q_y)$ is a Dirac delta function and Λ is a multiplying factor that accounts for the amplitude of the emitted signal. The Doppler spectrum is defined as the power spectrum of the real part of acoustic field U:

$$\widehat{U}(\boldsymbol{M},\boldsymbol{S},f) = \left|\frac{1}{T}\int_T Re[U(\boldsymbol{M},\boldsymbol{S},t)]e^{i2\pi ft}dt\right|^2 . \quad (3)$$

2.2 Surface dynamics

The spatial auto-correlation of the roughness function is defined as

$$C(\rho) = \frac{1}{\Sigma_0}\int_{\Sigma_0} < \zeta^*(x-\rho,t)\zeta(x,t) > dx \ , \quad (4)$$

where ρ is the spatial separation between the points that are being correlated and the asterisk suffix represents the complex conjugate. The correlation function relates to the spatial spectrum of the rough surface $\hat{Z}(k_w)$ by

$$C(\rho) = \frac{1}{2\pi}\int_{-\infty}^{\infty}\hat{Z}(k_w)e^{ik_w\rho}dk_w \ . \quad (5)$$

The surface roughness pattern of the free surface of a shallow flow are believed to originate from the interaction with turbulent structures that are generated in the water flow, mainly at the channel bed[7]. The surface patterns above such turbulent structures are then advected at a constant velocity which is equal to the flow velocity close to the surface, U. Turbulent structures are able to interact with the free-surface for a limited period of time before their coherence diminishes due to dissipation. When the turbulent forcing vanishes, it is expected that the rough surface will be constituted by a mostly incoherent pattern of gravity-capillary waves. These waves are dispersive, and their dispersion relation can be approximated by the equation

$$\omega_w = \sqrt{\left(g + \frac{\gamma}{\rho}k_w^2\right)k_w\tanh(k_w h)} \quad , \quad (6)$$

where k_w and ω_w are the wavenumber and radian frequency of the waves respectively, g is the gravity constant, γ the surface tension coefficients, ρ is the density of water and h is the mean depth of water. The wave phase velocity is defined as $\boldsymbol{c_w} = \omega_w/\boldsymbol{k_w}$. Gravity waves are advected at the constant surface velocity U. Their effective phase velocity depends on their direction of propagation according to

$$V(k_w) = U + \boldsymbol{c_w}(k_w)\cdot\boldsymbol{i_x} \ . \quad (7)$$

2.3 Bragg scattering

Most of the literature regarding backscattering of electromagnetic waves from the rough sea surface concentrates on cases where the source and receiver are both in the Fraunhofer zone with respect to the surface, and where the amplitude of surface fluctuations is either very large or very small with respect to the wavelength of the incident wave. In this conditions most of the backscattered intensity comes from the interaction with surface waves which wavelength satisfies the Bragg condition

$$\lambda_b = \frac{2\pi}{k_b} = \frac{\lambda_o}{2cos\psi} \ . \tag{8}$$

These waves are expected to propagate along all different directions so that their phase velocity follows equation 7, where $\boldsymbol{c_w}(k_w) \cdot \boldsymbol{i_x} = \pm c_w(k_w)$ for the one-dimensional case. The frequency spectrum of the backscattered signal is then expected to show two peaks, one for the advancing ($V^+ = U + c_w(k_b)$) and one for the receding ($V^- = U - c_w(k_b)$) Bragg waves. An additional peak corresponding to the velocity $V^T = U$ is representative of the turbulence forced structures which are simply advected at the mean surface flow velocity. This defines the reference Doppler frequency shift $f_D = 2k_0 U cos\psi / 2\pi$. The relative amplitude of the characteristic peaks depends on the amplitude of the corresponding surface waves, and it is a function of their direction of propagation. For ocean waves that are generated by wind the so-called angular spreading function was studied thoroughly[8], while its determination is difficult in open channels where the mechanism of surface roughness generation by the interaction with the turbulent flow is still unquantified[3].

3 NUMERICAL MODEL

For most practical applications in open-channel flows, the source and the receiver need to be relatively close to the water surface in order for the backscattered signal to be strong enough to be detected. The Fraunhofer condition is hence often violated, and the directivity patterns of the source and receiver affect the resulting spectra significantly. Moreover, as the flow kinetic energy increases, the amplitude of surface fluctuations becomes comparable with the acoustic wavelength and the scattering equations must be solved exactly without simplifications.

The backscattering of ultrasonic waves from the moving water surface in open channels has therefore been modelled numerically by means of a Monte Carlo simulation. The surface has been represented as a one dimensional random function of the x co-ordinate only. Each surface realisation is the sum of three subsurfaces corresponding to the two sets of advancing and receding gravity-capillary waves and the forced components travelling at the constant flow surface velocity U:

$$\zeta = \zeta^+ + \zeta^- + \zeta^T \ . \tag{9}$$

Each m-th realization of the generic subsurface $\zeta^{(\cdot)}(x,t)_m$ has been generated as a cosine series with the phase $\varphi_n^{(m)}$ being drawn from a random homogeneous distribution in the interval $(0\ 2\pi)$

$$\zeta^+(x,t)_m = \sum_{n=1}^{N} \hat{A}(k_{w,n})\ \cos\left[k_{w,n}x - \omega^+(k_{w,n})t + \varphi_n^{(m)+}\right], \tag{10a}$$

$$\zeta^-(x,t)_m = \sum_{n=1}^{N} \hat{A}(k_{w,n})\ \cos\left[k_{w,n}x - \omega^-(k_{w,n})t + \varphi_n^{(m)-}\right], \tag{10b}$$

$$\zeta^T(x,t)_m = \sum_{n=1}^{N} \hat{A}(k_{w,n})\ \cos\left[k_{w,n}x - \omega^T(k_{w,n})t + \varphi_n^{(m)T}\right], \tag{10c}$$

where the dispersion relation for each subset of waves is given by the set of equations

$$\omega^{+}(k_{w,n}) = k_{w,n}U + \omega_w(k_{w,n}), \quad (11a)$$
$$\omega^{-}(k_{w,n}) = k_{w,n}U - \omega_w(k_{w,n}), \quad (11b)$$
$$\omega^{T}(k_{w,n}) = k_{w,n}U. \quad (11c)$$

The function $\hat{A}(k_w)$ corresponds to the spatial amplitude spectrum of the rough surface and its square modulus is proportional to the Fourier transform of the correlation function $\hat{Z}(k_w)$.

$$\hat{Z}(k_w) = \left|\hat{A}(k_w)\right|^2 . \quad (12)$$

It is believed that the behaviour of the dynamically rough surface and its spatial spectrum $\hat{A}(k_w)$ are directly linked to the mechanism of roughness generation. The characteristic power spectrum of waves generated by wind has been determined with good accuracy up to relatively short scales in the capillary range[8] which are fundamental for backscattering of high-frequency acoustic signals. This spectrum follows a power law function of the wavenumber k_w with an exponent α which represents the balance between the different phenomena that control the dynamics of the surface. The mechanisms by which waves are generated at the surface of a turbulent open-channel flow in absence of wind are still largely unknown and even the experimental characterization of the surface spectrum is challenging with the most common measurement techniques: time series of the surface elevation at a point cannot be converted to spatial frequencies because of the dispersive nature of gravity-capillary waves. In the laboratory environment arrays of conductance waveprobes can be used to determine the spatial characteristics of roughness, but their spatial resolution is limited by electric interference and by the number of channels that need to be recorded simultaneously. There are surface PIV and optical methods which have good resolution but over a relatively small aperture. None of these techniques seems to be able to reliably and accurately characterize the small scales of roughness associated with shallow flows which contribute to the backscattering of high frequency sound. In this paper we assume a simple shape of the surface spectrum in the form

$$\hat{A}(k_w) = \sqrt{\hat{Z}(k_w)} = \begin{cases} \hat{A}_0 & when\ |k_w| \le k_c \\ \hat{A}_0 \left(\frac{k_w}{k_c}\right)^{-\alpha/2} & when\ |k_w| > k_c \end{cases}, \quad (13)$$

where k_c corresponds to a characteristic scale $\lambda_c = 2\pi/k_c$ and $\hat{A}_0$ is a scaling factor which represents the characteristic amplitude of longer waves. $\hat{A}_0$ is determined so that the standard deviation of roughness at the initial instant matches the average measured standard deviation:

$$\sqrt{\frac{1}{L}\int_L [\zeta(x,0)]^2 dx} = \sigma . \quad (14)$$

The value of α was determined after some preliminary numerical simulations. Figure 1a shows the estimated Doppler spectrum for the flow regime with $h = 70\ mm$ and tangent bed slope 0.001, for different choices of the exponent α. The best fit with the experimental data is obtained when α is between 2 and 3. These are much lower values than the one that was measured by Savelsberg and Van De Water[9] for grid-induced turbulence in a shallow open-channel flow. We choose the value of $\alpha = 2$ and substitute equation 13 into equation 5. This allows defining an analytical form of the auto-correlation function, say $C_\alpha(\rho, k_c)$, as the inverse Fourier transform of the ideal surface spectrum $\hat{Z}(k_w)$. $C(\rho)$ was measured experimentally with an array of conductance waveprobes at various spatial separations, so that the optimal value of k_c could be determined by fitting the experimental measurements with the function $C_\alpha(\rho, k_c)$ in a least-square sense. Substituting equations 13 and 11 into equations 10 allows for generating random realizations of the dynamic surface ζ which are then used in order to estimate the backscattered field according to equations 2 and 3.

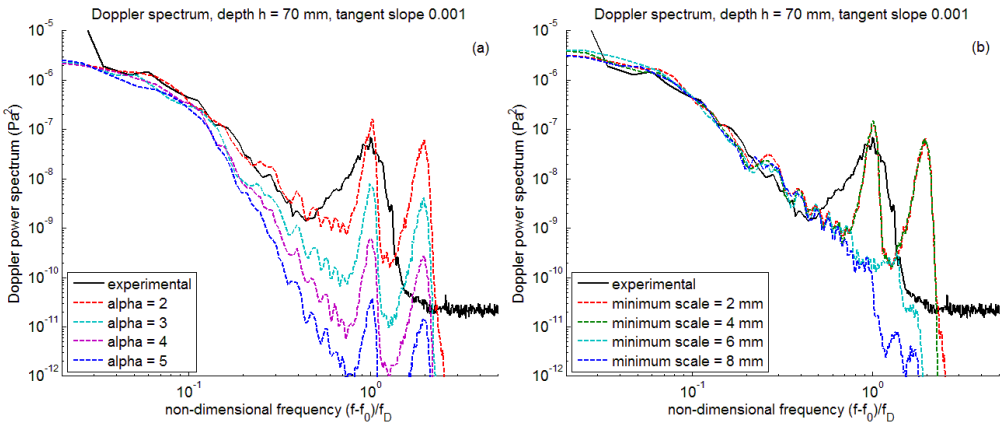

Figure 1: measured Doppler spectrum for $h = 70\,mm$, tangent slope of 0.001, compared to numerical model predictions. (a) effect of the surface roughness spectrum exponent, α; (b) effect of the spectrum cut-off at small scale λ_{min}.

4 EXPERIMENTAL MEASUREMENTS

Measurements were collected in an open-channel flume which is 12.6 m long and 0.459 m wide, with a rectangular section. It allows fine control on the flow discharge, and can be tilted so to obtain the desired combination of uniform flow depth (within 20 mm and 130 mm) and flow velocity (up to 0.6 m/s). The tangent slope of the channel can be varied between 0.001 and 0.006. Uniform flow conditions were ensured by an adjustable gate at the outlet end of the channel, and monitored with a set of point gauges distributed at different locations along the centreline of the channel. At the time of measurements, the bed of the channel was covered with two dense layers of hexagonally packed plastic spheres, each with a diameter of 25.4 mm. The velocity at the surface, U, was measured by dropping neutral buoyancy particles on the flow surface several times and timing their passage with optical means across a distance of 1.5 m.

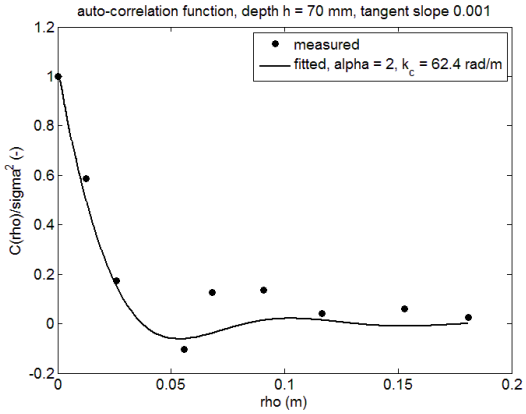

Figure 2: Measured spatial auto-correlation function for $h = 70\,mm$, tangent slope of 0.001. Experimental data obtained with the array of conductance waveprobes (dots) are fitted with a curve that represents the inverse transform of the hypothetic surface spectrum according to Equations 5, 12, and 13.

An array of conductance wave probes was installed at approximately 9 m from the inlet to measure the instantaneous surface roughness elevation at a range of positions. The auto-correlation function for the tested regimes was determined from the time records of the array of 8 irregularly spaced conductance waveprobes aligned along the flume centreline. The spacing between consecutive probes varied between 10 mm and 250 mm and it was chosen so to maximize the array measurement length and simultaneously minimize the gaps of the correlation array.

The acoustic setup consisted of a 70 mm diameter ultrasonic transducer (ceramic type 043SR750) and one B&K ¼" 4939-A-011 laboratory microphone. The source was located approximately 8 m downstream from the flume inlet. It was suspended at a vertical distance of 200 mm from the mean water surface and inclined by $\psi_0 = 30$ ° with respect to the horizontal plane facing the upstream end of the flume. The microphone was inclined parallel to the source main axis and placed so that its membrane was located 50 mm below and 28 mm behind the centre of the source. The directivity polar pattern of the acoustic source D_S has been characterised in an anechoic room at a distance of 250 mm from the source, varying the inclination angle from 0 ° to 360 ° with steps of 2.5 °. The microphone directivity was estimated according to factory specifications. The source was energised with a continuous 10 V peak-to-peak amplitude harmonic signal at a frequency of $f_0 = 43\ kHz$. The backscattered signal recorded by the microphone was initially conditioned with a Nexus type 2690 conditioning amplifier and later digitised and processed with a National Instrument PXIe acquisition system. The signal was sampled at a frequency of $f_s = 500\ kHz$ in segments of 1 second length and then filtered with a second order Butterworth bandpass filter between the frequencies $0.9f_0$ and $1.1f_0$. Each filtered segment was windowed with a Hanning function in time, and the amplitude spectrum was estimated by means of an FFT. The Doppler spectrum representative of a flow regime was then taken as the average power spectrum across 50 separate segments of 1 second each.

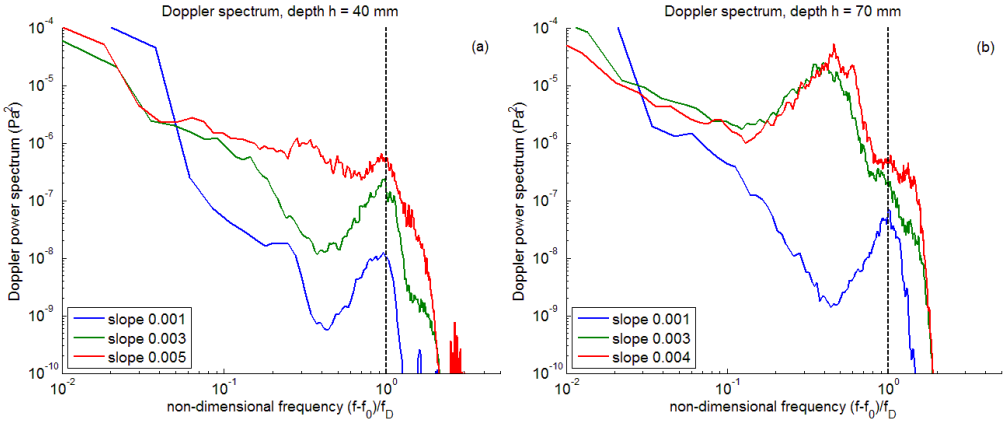

Figure 3: Measured Doppler spectra. (a) $h = 40\ mm$, tangent slope from 0.001 to 0.005; (b) $h = 70\ mm$, tangent slope from 0.001 to 0.004. The dashed line at $f = f_D$ corresponds to the reference Doppler shift computed for the mean flow velocity $f_D = 2k_0 U cos\psi_0 / 2\pi$.

Figure 3 shows the measured Doppler spectra for the different regimes that have been tested, in which each separate graph represents all measurements made with the same mean water depth. The x-axis of all graphs have been non-dimensionalised by subtracting the carrier frequency and dividing the remainder by the reference Doppler shift $f_D = 2k_0 U cos\psi_0 / 2\pi$. All spectra are continuous and smooth, with a predominant component at very low non-dimensional frequency, i.e. at a frequency very close to the carrier. This component derives from sound waves that reflect almost perpendicularly towards the surface and it clearly dominates the spectra in spite of the narrow directivity pattern. A spectral peak can be noticed at higher frequency and in particular close to the frequency f_D. This peak represents the turbulence induced surface patterns that follow the turbulent structures at a velocity equal to the mean flow velocity. The slowest regimes with the slope of 0.001 display a single relatively narrow peak at the frequency f_D. As the slope (and the flow velocity) is increased there is a rise of the spectral components at lower and higher frequency with respect to f_D, and in particular within the interval between $2k_0 V^-(k_b) cos\psi_0 / 2\pi$ and $2k_0 V^+(k_b) cos\psi_0 / 2\pi$. These additional components represent advancing and receding capillary waves whose absolute velocity is larger and smaller than U, respectively. Receding waves seem to have larger impact on the Doppler spectra, and they eventually become larger than the turbulence generated component at the higher slopes.

The choice of the acoustic signal and angle of incidence determines the wavelength of Bragg resonant waves $\lambda_b = \lambda_0/(2cos\psi_0) = 4.6\,mm$. The dynamics of these short capillary waves are controlled mainly by surface tension effects. The impact of Bragg resonance on the acoustic backscattering is demonstrated in figure 1b, which shows the predicted Doppler spectra relative to the regime with the depth of $h = 70\,mm$ and the tangent slope of 0.001. These spectra were obtained with the numerical model described in §2, where the spectrum of equation 13 has been truncated at a minimum scale λ_{min} which was let vary between $2\,mm$ and $8\,mm$. The relatively narrow frequency-shifted peaks are all associated with Bragg scales with wavelength between $4\,mm$ and $6\,mm$, including the central peak at the reference frequency f_D. The low-frequency portion of the spectrum is associated with larger scales and the only apparent effect of truncating the surface spectrum is to move the Doppler spectrum cut-off to lower frequency. This suggests the existence of a direct link between the spectrum of the free-surface and the spectrum of the backscattered acoustic signal.

5 MODEL RESULTS

The model presented in §3 was used in order to generate random realisations of the flow surface with the same properties of the experiments. Measured auto-correlation functions like the one shown in Figure 2 were used to determine the value of k_c which gives the best fit to the ideal surface spectrum of equation 13. The instantaneous surface realisations were obtained according to equations 9 and 10 for x that was varied from $-0.5\,m$ to $0.5\,m$ from the point of the maximum in the directivity of the projected sound wave. For each realisation, the acoustic field was determined by solving equation 2 numerically at every time steps while the time variable was increased in steps of $1\,ms$ for a total time period of $1\,s$. $U(\boldsymbol{S}, \boldsymbol{M}, t)$ was then used to estimate the Doppler spectrum of a single realisation according to equation 3. The representative Doppler spectrum for one particular flow regime was taken as the average of the corresponding spectra over 50 realisations. The results for some characteristic flow regimes are shown in Figure 4.

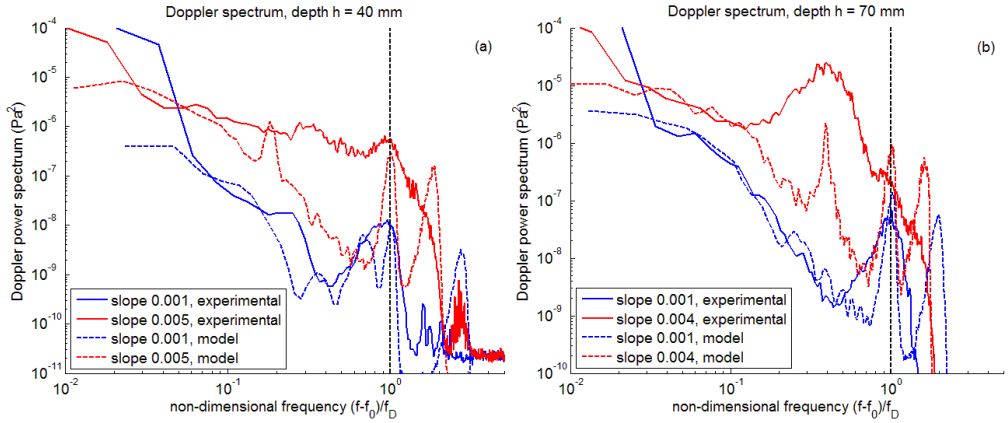

Figure 4: measured Doppler spectra (solid lines) against predictions of the one-dimensional model (dashed lines): (a) $h = 40\,mm$, tangent slope 0.001 and 0.005; (b) $h = 70\,mm$, tangent slope 0.001 and 0.004.

Because of the many assumptions on the free-surface geometric and dynamic characteristics, the matching between the measured and predicted Doppler spectra is purely qualitative. The Doppler spectra that are predicted by the model are characterised by narrow peaks corresponding mainly to the velocity of capillary waves which satisfy the Bragg resonance condition. Measured Doppler spectra generally display broader peaks, which could be a consequence of non-linear interaction between water waves with different scale[10]. The impact of the advancing waves on the measured spectrum is always overestimated by the model, while receding waves are underestimated in the flow regime with $h = 70\,mm$ and tangent slope of 0.004. The relative amplitude of the different contributions to the spectrum depends on the directional spectrum of the free-surface, which was

assumed to be independent on the direction of propagation in this simple model. The hypothesis of the surface spectrum to follow a power law with exponent $\alpha = 2$ leads to a shape of the modelled Doppler spectra which seems consistent with the measured data, especially at low frequency. The model predicts well the cut-off of the Doppler spectra at high frequency, which depends on the velocity of the advancing capillary waves. It also recognizes the advent of receding waves when their absolute velocity $V^- = U - c_w(k_b)$ becomes positive.

6 CONCLUSIONS

The Doppler spectra of airborne ultrasonic waves backscattered by the dynamically rough free-surface of shallow, open-channel flows have been presented for a range of flow regimes. The measured spectra reveal the nature of the rough flow surface, which is constituted of waves travelling at the mean flow velocity and of a more complex pattern of gravity-capillary waves which are dispersive. The relative amplitude of the different components of the surface roughness is dependent on the flow conditions, and it is difficult to characterise or predict.

The problem of scattering of sound from the moving water surface has been modelled numerically in one dimension assuming that the surface spectrum follows a power law function with exponent $\alpha = 2$. Because the exact directional spectrum of waves had to be assumed, the comparison between the modelled and measured Doppler spectra can only be approached from a qualitative point of view. The experimental Doppler peaks are generally broader, which suggests that two-dimensional effects and non-linear effects may be non-negligible. The main contributions to the spectrum coming from different types of waves are all correctly described by the model, although their relative magnitude depends on the flow conditions in a way that is difficult to interpret. Future investigation will be devoted to trying different types of surface spectra introducing the dependence on the direction of propagation, with the aim of gaining a better fit with the experimental data and of improving the current knowledge of the free-surface dynamics in shallow flows.

7 REFERENCES

1. L.R. Wyatt, ‘Operational wave, current, and wind measurements with the Pisces HF radar, IEEE J. Oceanic Eng. 31(4) 819-834. (2006).
2. J.E. Costa, et al., ‘Use of radars to monitor stream discharge by noncontact methods’, Water Resour. Res. 42 W07422. (2006).
3. W.J. Plant, W.C. Keller and K. Hayes, ‘Measurement of river surface currents with coherent microwave systems’, IEEE Trans. Geosci. Rem. Sens. 43(6) 1242-1257. (2005).
4. M.C. Lee, et al., ‘Non-contact flood discharge measurements using an X-band pulse radar (I) Theory’, Flow Meas. Instrum. 13(5) 265-270. (2002).
5. C.J. Wang, et al., ‘Measurement of river surface currents with UHF FMCW radar systems’, J. Electromagn. Waves Appl. 21(3) 375-386. (2007).
6. F.G. Bass and I.M. Fuks. Wave Scattering from Statistically Rough Surfaces. Oxford, Pergamon Press. (1979).
7. I. Fujita, Y. Furutani and T. Okanishi, ‘Advection features of water surface profile in turbulent open-channel flow with hemisphere roughness elements’, Visual. Mech. Process. 1(4). (2011).
8. T. Elfouhaily, et al., ‘A unified directional spectrum for long and short wind-driven waves’, J. Geophys. Res. (Oceans) 102(C7) 15781-15796. (1997).
9. R. Savelsberg and W. Van De Water, ‘Experiments on free-surface turbulence’, J. Fluid Mech, 619 95-125. (2009).
10. J.T. Johnson, J.V. Toporkov and G.S. Brown, ‘A numerical study of backscattering from time-evolving sea surfaces: Comparison of hydrodynamic models’. IEEE Trans. Geosci. Rem. Sens. 39(11) 2411-2420. (2001).